



Direct Synthesis of H₂O₂

How to cite: Angew. Chem. Int. Ed. 2025, e21118 doi.org/10.1002/anie.202521118

Direct Synthesis of H₂O₂ by Spatially Separate Hydrogen and Oxygen Activation Sites on Tailored Pt–Au Catalysts

Ying Zhang⁺, Richard J. Lewis⁺, Zhichao Li, Xiaohui He,* Hongbing Ji,* and Graham J. Hutchings*

Abstract: The direct synthesis of H_2O_2 is considered an atom-efficient, environmentally friendly, and sustainable alternative to replace the current industrial route of the anthraquinone oxidation process. To date a viable direct replacement for the current industrial method of H_2O_2 production has yet to emerge, owing to the strong dissociation abilities of traditional Pd-based catalysts for both H_2 and O_2 , which results in the over hydrogenation of H_2O_2 and limited catalytic activity. To address these concerns, this work outlines a novel non-Pd-based catalyst (Pt₁Au_n/TiO₂), consisting of spatially separated H_2 and O_2 activation sites, which offers H_2O_2 selectivity ($\sim 100\%$) and productivity (128.6 mol·g_{N.M.} $^{-1}$ ·h $^{-1}$), in excess of state-of-the-art formulations. Crucially, via consecutive reactions, this system achieves net H_2O_2 concentrations approaching 4 wt.%, which is double that generated in the initial stages of the Anthraquinone Oxidation Process. A detailed mechanistic study indicates that Pt single atoms selectively dissociate H_2 , while Au nanoparticles stabilize non-dissociative *O_2 species. The H_2O_2 formation proceeds through CH_2O -mediated hydrogen transfer, generating a hydrogen carrier (*CH_2OH) that subsequently reacts with *O_2 to produce H_2O_2 .

Introduction

Hydrogen peroxide (H₂O₂), recognized as one of the most vital global chemicals, holds immense economic significance, with approximately 50% of global H₂O₂ production dedicated to bulk chemical synthesis, while also playing critical roles in sectors as far-ranging as medical disinfection, bleaching, wastewater treatment, and emerging energy technologies.^[1-4] As an environmentally benign oxidant, H₂O₂ decomposes exclusively into water and oxygen, offering a sustainable alternative to traditional stoichiometric oxidants.^[5,6] This unique combination of high efficiency and environmental

compatibility has driven a steady rise in global demand.^[7] Currently, industrial production of H₂O₂ relies wholly on the anthraquinone oxidation (AO) process, which generates H₂O₂ through cyclic hydrogenation and oxidation of an anthraquinone carrier, followed by energy-intensive purification and extraction steps.^[8] However, this method suffers from inherent drawbacks, including the need for high capital investment, incomplete atom efficiency, environmental and safety concerns, and the generation of large quantities of greenhouse gases.[9,10] Moreover, to reduce transport and storage costs, H₂O₂ is typically shipped at concentrations (30– 70 wt.%) far exceeding the requirements of most applications (<9 wt.%), necessitating dilution steps at the point of use and effectively wasting the energy utilized in earlier extraction steps.[11,12] The inherent instability of H₂O₂, which is prone to rapid decomposition, further mandates stringent temperature control and the use of proprietary stabilizing agents, which often promote reactor corrosion and generate complex product streams.

As a promising route toward sustainability, the direct synthesis of H₂O₂ (DSHP) has garnered significant attention for over 100 years due to its environmental compatibility, potential for cost efficiency, and on-demand production. [13,14] However, poor catalytic selectivity, resulting in the formation of H₂O (either through combustion of H₂ and O₂ or the decomposition and hydrogenation of H₂O₂), has until recently been a major hurdle to industrial adoption. In recent years, several catalyst formulations that achieve > 95% selectivity have been reported, [1,4,15,16] and while issues of catalytic selectivity are still considered a primary challenge to the upscaling of any direct approach, significant improvements in catalytic reactivity are also required if the direct approach is to rival the AO Process. [17] Particularly, economic viability can

[*] Dr. Y. Zhang⁺, Z. Li, Prof. X. He, Prof. H. Ji Key Laboratory of Bioinorganic and Synthetic Chemistry of Ministry of Education, Fine Chemical Industry Research Institute, School of Chemistry, IGCME, Sun Yat-Sen University, Guangzhou 510275, China

E-mail: hexiaohui@mail.sysu.edu.cn jihb@mail.sysu.edu.cn

Dr. R. J. Lewis⁺, Prof. G. J. Hutchings Max Planck–Cardiff Centre on the Fundamentals of Heterogeneous Catalysis FUNCAT, Cardiff Catalysis Institute, School of Chemistry, Cardiff University, Cardiff CF24 4HQ, UK E-mail: hutch@cardiff.ac.uk

Prof. H. Ji

State Key Laboratory Breeding Base of Green-Chemical Synthesis Technology, Institute of Green Petroleum Processing and Light Hydrocarbon Conversion, College of Chemical Engineering, Zhejiang University of Technology, Hangzhou 310014, P. R. China

- [+] Both authors contributed equally to this work.
- Additional supporting information can be found online in the Supporting Information section

only be achieved if net H_2O_2 concentrations offered by the DSHP can rival that generated in the initial stages of the AO Process (\sim 2 wt.%).^[18]

Pd-based catalysts have been widely reported to exhibit high activity for H₂O₂ synthesis. However, the strong dissociative ability of Pd towards O2 promotes H2O formation, thereby significantly reducing both H₂O₂ selectivity and productivity. Meanwhile, the presence of active hydrogen species and freshly synthesized H₂O₂ on Pd surfaces often triggers the over-hydrogenation of H₂O₂. [4,19] To address these limitations, researchers have typically relied on the use of halide and acid promoters to inhibit side reactions,[20,21] and have more recently developed a variety of strategies, including the incorporation of secondary metals,[1,15,22-25] the construction of confined structures, [26,27] and ligand modification^[28-31] to tailor the geometric and electronic structure of Pd sites, to inhibit H₂O formation. Although these approaches have improved catalytic performance, Pdbased catalyst systems still face unresolved challenges, leading to H₂O₂ concentrations that remain incomparable to those achieved by the AO Process.[32]

Notably, research on non-Pd-based catalysts has received scant attention,[33] which likely stems from the poor dual activation capability for both H2 and O2 of alternative metal species, leading to inadequate activity, selectivity, and stability.[34-38] For instance, PtAu nanoalloys have been reported to offer only moderate H₂O₂ selectivity (36%–85%), while activities are extremely low (the productivity is only $\sim 0.07 \text{ mol} \cdot g_{\text{N.M.}}^{-1} \cdot h^{-1}$, N.M. is short for noble metals), much lower than those of the Pd-based catalysts. [36,37] Furthermore, the incomplete understanding of active sites and H₂O₂ formation mechanisms in both Pd- and non-Pd-based catalyst systems remains a persistent challenge for advancing their practical implementation in DSHP. Considering that in the case of conventional DSHP catalysts, both the activation of H₂ and O₂ occur on the same metal sites, [39,40] there is perhaps understandable difficulty in separately controlling the dissociative adsorption of H₂ and non-dissociative adsorption of O_2 .

Herein, we propose an innovative strategy to decouple these two key activation processes and assign them to distinct metal sites, thereby substantially enhancing the efficient synthesis of H₂O₂. A non-Pd-based catalyst (Pt₁Au_n/TiO₂) with high H₂O₂ synthesis performance is constructed, which features spatially separated Pt single atoms (SAs) and Au nanoparticles (NPs) discretely anchored on TiO₂. The catalyst offers ~100% H₂O₂ selectivity and improves upon the productivity of non-Pd-based catalysts by 2-3 orders of magnitude. Notably, H₂O₂ concentrations approaching 4 wt.% are achieved after 10 reaction cycles, which is 3.6 times that of the best Pd-based catalyst and offers compatibility with purification and extraction processes downstream of industrial production. The catalytic mechanism involves H₂ activation/dissociation on Pt SAs to form *H+, and O2 nondissociative adsorption on Au NPs to form *O₂⁻, with CH₂Omediated hydrogen transfer facilitating the combination of *H⁺ species with *O₂⁻ species, ultimately enabling highly efficient H₂O₂ synthesis.

Results and Discussion

Catalysts Synthesis and Catalytic Performance

We initially prepared a series of bimetallic catalysts comprising Pt and a range of secondary metals on a TiO₂ support using a ball milling method (for details see Experimental Section), denoted as PtM/TiO₂ (M = Au, Pd, Ir, Ru, Rh, Ag, Fe, Co, Ni, and Cu). Metal loadings were confirmed by the inductively coupled plasma optical emission spectrometry (ICP-OES, Table S1), which indicated that the Pt content was \sim 0.2 wt.% and the second metal content was \sim 0.8 wt.%. Analysis by transmission electron microscopy (TEM) and scanning transmission electron microscopy (STEM) revealed that these catalysts featured a similar geometric structure (NPs sizes of \sim 2.0 nm, Figures S1–S10). In a typical DSHP reaction (Figures 1a and S11, reaction conditions: 10 mL CH₃OH, 2.9 MPa 5% H₂/N₂, 1.1 MPa 25% O₂/N₂, T = 0 °C, 5 mg catalyst, 10 min, and stirring: 1200 rpm), only the PtAu, PtPd, PtIr, PtRu, and PtRh catalysts demonstrated any H₂O₂ formation activity. Interestingly, the PtAu catalysts (denoted as Pt₁Au_n/TiO₂) showed superior catalytic performance (H₂ conversion of 11.8%, H₂O₂ selectivity of 99.6%, and a H₂O₂ productivity of 45.1 mol· g_{NM}^{-1} ·h⁻¹), significantly outperforming the remainder of the catalyst series (H2O2 selectivity < 18%, the H_2O_2 productivity < 10 mol· g_{NM} ⁻¹·h⁻¹). We further prepared a series of Au-containing bimetallic catalysts (MAu/TiO₂ catalysts, M = Pd, Ir, Ru, Rh, Ag, Fe, Co, Ni, and Cu) by an identical ball milling procedure, achieving catalysts consisting of similar structures and metal content (Table S2 and Figures S12-S20). However, apart from the PtAu/TiO₂ catalyst, the generation of H₂O₂ was observed only over the Pd-containing analogue (H2 conversion of 9.3% and H₂O₂ selectivity of 32.6%), but notably, H₂O₂ productivity (12.4 mol·g_{NM} ⁻¹·h⁻¹) was only one-fourth that of the Pt₁Au_n/TiO₂ catalyst (Figures 1b and S21). Indeed, compared to previously reported formulations (Figure 1c and Table S3), the Pt₁Au_n/TiO₂ catalyst, without adding any promoters, offered H₂O₂ productivity in excess of 56 times that of the most active non-Pd-based catalyst (AgPt/SiO₂, 0.8 mol·g_{N.M.}⁻¹·h⁻¹),^[35] and comparable to the state-of-theart Pd-based catalysts (0.1%O-Pd/TiO₂, 115 mol·g_{N.M.}⁻¹·h⁻¹, with CO₂ as an in situ promoter)^[4] under the identical H₂ conversion (\sim 3.5%, the corresponding H_2O_2 productivity on our Pt_1Au_n/TiO_2 was 128.6 mol· $g_{N.M.}^{-1}\cdot h^{-1}$).

The impact of H_2/O_2 ratio on catalytic performance was further investigated (Figure S22), with these studies demonstrating that the Pt_1Au_n/TiO_2 catalyst exhibited exceptional performance (>99% H_2O_2 selectivity) across a wide range of H_2 concentrations (1.6–3.6 vol.%). The choice of solvent has been well reported to be a critical factor in determining catalytic performance in DSHP, demonstrating that the promotive effects that resulted from the use of alcohol-based (and other protic) solvents may be attributed to the direct involvement of the solvent within the mechanism where H_2O_2 was formed by a proton- (from solvent molecules) electron (provided by heterolytic hydrogen oxidation) transfer to surface-bound intermediates.^[41] Aligning with this work, we

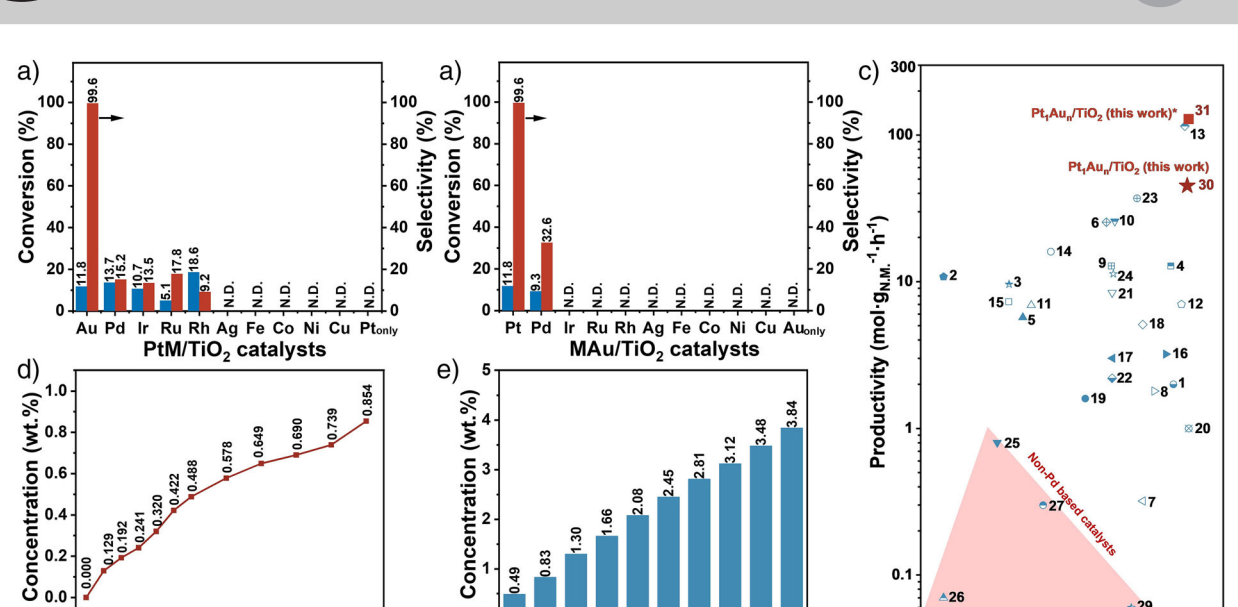


Figure 1. Comparative H2 conversion and H2O2 selectivity on a) Pt1/TiO2 and PtM/TiO2 (M = Au, Pd, Ir, Ru, Rh, Ag, Fe, Co, Ni, and Cu) catalysts, b) Au_n/TiO₂ and MAu/TiO₂ (M = Pt, Pd, Ir, Ru, Rh, Ag, Fe, Co, Ni, and Cu) catalysts for DSHP. N.D.: no H₂ conversion were detected. Reaction condition: 10 mL CH₃OH, 2.9 MPa 5% H₂/N₂, 1.1 MPa 25% O₂/N₂, T = 0 °C, 5 mg catalyst, 10 min, and stirring: 1200 rpm; c) H₂O₂ productivity and selectivity for the catalysts described in this work and References from Table S3 in Supporting Information. Note, the productivity was calculated based on the noble metal contents, N.M.: noble metals. The productivity and selectivity on Pt_1Au_n/TiO_2 represented by (\blacksquare) and (*) were obtained at H₂ conversion of 3.2% and 11.8%, respectively; d) H₂O₂ concentration as a function of reaction time on Pt₁Au_n/TiO₂; e) Sequential H₂O₂ synthesis reactions using Pt_1Au_n/TiO_2 , 30 min for every reaction with the H_2 conversion at \sim 45%.

established the high dependence of catalytic performance on the choice of solvent (Figure S23), with $\sim 10\%$ H₂ conversion and > 99% H₂O₂ selectivity achieved when using pure CH_3OH as the solvent, while a H_2O , $70\%CH_3OH + 30\%H_2O$ co-solvent, or C₂H₅OH only system offered lower activity, which may suggest that CH₃OH was directly involved in the reaction mechanism (discussed below). When extending the reaction time to 80 min (Figures 1d and S24), the H₂O₂ concentration increased linearly to 0.85 wt.%, accompanied by an 89.4% H₂ conversion, a productivity of 25.2 mol·g_{N,M}.⁻¹·h⁻¹, and a H₂O₂ yield of 52.5%. However, the H₂O₂ selectivity remained relatively stable at around 60%, which may be caused by the partial reduction of Pt species (the proportion of Pt²⁺ decreased from 100% to 81%) upon exposure to the reaction conditions, as evidenced by X-ray photoelectron spectroscopy (XPS, Figure S25), while the geometric structure remained substantially unchanged (Figure \$26). Analysis of the post-reaction solution by the inductively coupled plasmamass spectrometry (ICP-MS) revealed the relative stability of the catalyst after reaction for 30 min, with a negligible loss of Pt (0.11%) and Au (0.07%) observed. Finally, we observed that H₂ conversion reached 45.5% after 30 min (Figure S24A). In order to avoid the potential for mass transfer limitations, sequential H₂O₂ synthesis reactions were conducted every 30 min through the replacement of gaseous reagents. The results in Figure 1e indicated a nearly linear increase in H₂O₂ concentration, which reached 3.84 wt.% after 10 reaction cycles, far exceeding the state-of-the-art Pd-based catalysts (1.07 wt.%, 0.1%O-Pd/TiO₂, Table S3).^[4] Notably, this concentration was twice as high as that produced

30 40 50

Time (min)

20

60

in the initial stages of the industrial approach to H₂O₂ production (~2 wt.%),[18] and as such overcomes a major hurdle, associated with any prior investigation into the direct synthesis approach, namely the high energy costs associated with the concentration of H₂O₂ streams to levels feasible for some practical applications.

0.1

30 40 60 70

50

90

80 Selectivity (%)

Insights to the activation sites

In order to obtain specific structural information regarding Pt and Au speciation, we conducted analysis by spherical aberration-corrected high-angle annular dark field scanning transmission electron microscope (AC HAADF-STEM) and X-ray absorption spectroscopy (XAS) on the as-prepared Pt₁Au_n/TiO₂ catalyst. Analysis by AC HAADF-STEM (Figures 2a and S27) revealed numerous Pt SAs uniformly dispersed around Au NPs, which was further supported by energy dispersive spectrometry (EDS, Figure 2b). The Pt L₃-edge X-ray absorption near-edge structure (XANES) spectrum suggested that Pt species in Pt₁Au_n/TiO₂ were cationic (Figure 2c). The Fourier transform (FT) k2-weighted extended X-ray absorption fine structure (EXAFS, Figure 2d) in R space showed an apparent peak at 1.6 Å assigned to Pt-O coordination, with no Pt-Pt bonding observed, demonstrating that the Pt species existed as SAs on the surface of TiO₂. [42] These results were also supported by the k-space spectrums, wavelet transform (WT), and fitting parameters (Figures S28–S30 and Table S4). The Pt–O in coordination number (CN) was 4.8 ± 0.7 , and the bond length was 2.1 ± 0.02 Å.

15213773, Q. Downloaded from https://onlinelibrary.wiley.com/doi/10.1002/anie.202521118 by Cardiff University, Wiley Online Library on [24/11/2023]. See the Terms and Conditions (https://onlinelibrary.wiley.com/retrms-and-conditions) on Wiley Online Library for rules of use; OA articles are governed by the applicable Creative Commons Licenses

Research Article

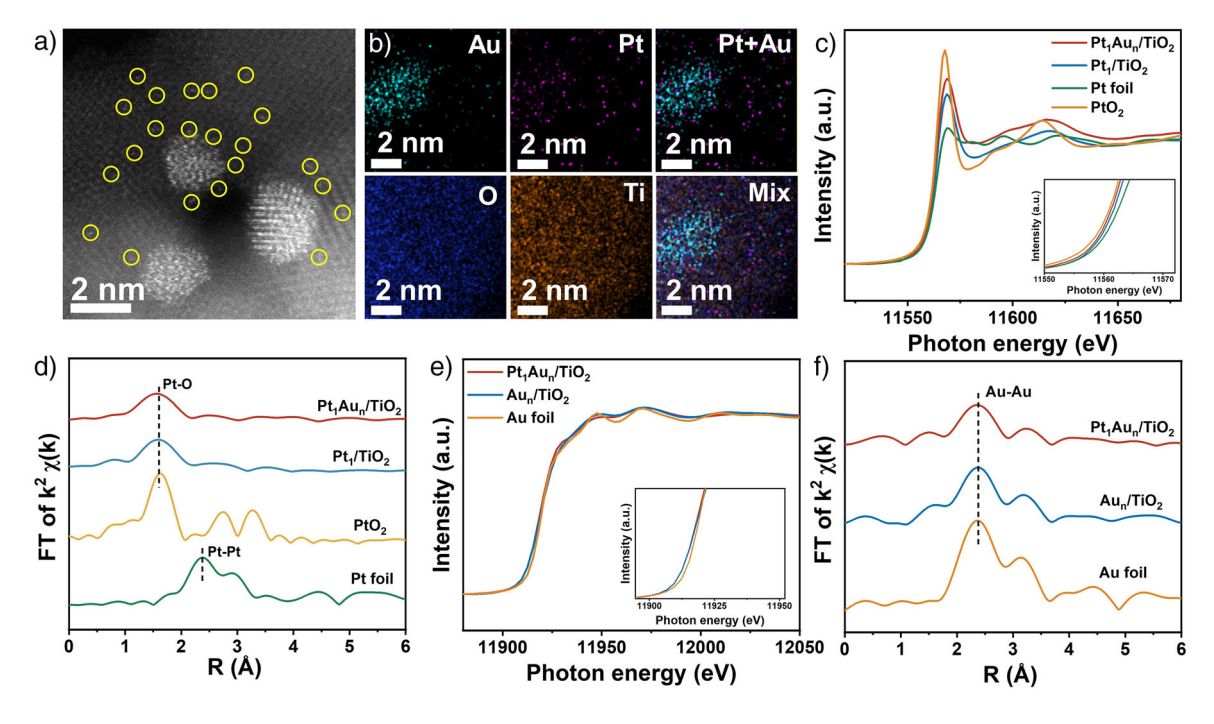


Figure 2. a) AC HAADF-STEM image, Pt single atoms are highlighted by the yellow circles. b) EDS mapping of Pt₁Au_n/TiO₂; c) Pt L₃ edge XANES profiles in R space; d) Pt EXAFS spectra; e) Au L₃ edge XANES profiles in R space; f) Au EXAFS spectra.

Further investigation by in-situ diffuse reflectance infrared Fourier transform spectroscopy of CO adsorption (CO-DRIFTS, Figure S31) showed a distinct CO adsorption peak at 2058 cm⁻¹, which was attributed to the linear adsorption of CO on cationic Pt SAs, [43] consistent with the XAS results. The XANES (Figure 2e), k-space spectrums (Figure S32), and WT (Figure \$33) of Au L₃-edge in Pt₁Au_n/TiO₂ were similar to that of Au foil, and the EXAFS (Figure 2f) showed only Au–Au coordination at 2.4 Å, indicating that Au species dispersed as NPs.[44] The fitting results revealed the CN of 9.3 ± 3.3 and bond length of 2.9 ± 0.02 Å (Figure S34 and Table \$5). For comparison, Pt₁/TiO₂ and Au_n/TiO₂ were successfully synthesized and verified by AC HAADF-STEM and EDS mapping (Figures 3a,b, with metal content reported in Table S6). XAS and CO-DRIFTS results (Figures 2c-f, S28-S34, Tables S4, and S5) revealed that Pt species in the Pt₁/TiO₂ catalyst were present as dispersed SAs, with Pt-O CN of 5.1 ± 1.2 and bond length of 2.0 ± 0.02 Å. In contrast, the Au species in Au_n/TiO₂ dispersed as NPs, with Au-Au CN of 10.4 ± 3.0 and bond length of 2.9 ± 0.02 Å.

To optimize the Pt/Au ratio, we prepared a series of PtAu/TiO₂ catalysts by varying Au content and fixing the Pt content at ~ 0.2 wt.% (as shown in Figures S35–S38 and Table \$7). As the Au content increased from 0.21 wt.% to 1.95 wt.% (i.e., the Pt/Au ratio increased from 1:1 to 1:10), H₂ conversion gradually increased from 6.7% to 28.0%. However, the selectivity was maintained at ~100% when the Pt/Au ratio was between 1:1 and 1:5, and decreased to 65.8% when increased to 1:10 (Figure \$39). To investigate the underlying mechanism, the dispersion and speciation of Pt and Au active sites were examined using AC HAADF-STEM and XPS. As shown in Figure \$40, increasing the Au content led to the gradual migrating of Pt into the

Au NPs (confirmed by the EDS results in Figure \$41). Indeed, at a Pt/Au ratio of 1:10, only a small number of Pt SAs were observed, corresponding with considerable alloy formation (Figure S42). Subsequent XPS analysis (Figure S43) confirmed that, as the Au content increased, the binding energy of Au 4f remained relatively constant at 83.2 eV, indicating that Au was in its metallic state. [45] However, the valence state of Pt was strongly influenced by the Au content. At low Pt/Au ratios (1:1 to 1:5), Pt species were positively charged (the binding energy of 72.9 eV), while a weak peak at 71.4 eV, corresponding to Pt⁰ species, [46] appeared at a Pt/Au ratios of 1:7 and 1:10, consistent with the AC HAADF-STEM analysis, which revealed the intimate mixing of metal species at these higher ratios. These observations were also confirmed by CO-DRIFTS analysis (Figure S31). A series of PtAu/TiO₂ catalysts were also prepared by varying Pt content and fixing the Au content at \sim 1 wt.% (Figures S44–S46 and Table S7). AC HAADF-STEM images indicated that PtAu alloys form as the Pt content reached 0.4 wt.%, aligning well with XPS and EDS analysis (Figures S47–S49). Increasing the Pt content from 0.09 to 0.90 wt.% (i.e., the Pt/Au ratio decreased from 1:10 to 1:1) led to higher H_2 conversion (9.9% to 24.7%). The selectivity remained $\sim 100\%$ at Pt/Au ratios of 1:10 and 1:5, but decreased to 40.2% when the ratio was reduced to 1:1, along with a decline in productivity (Figure \$50). These results demonstrated that the optimal performance was achieved at a Pt/Au ratio of 1:5 (i.e., Pt₁Au_n/TiO₂, the Pt content was 0.19 wt.% and the Au content was 1.0 wt.%), which could be attributed to the unique structure consisting of both positively charged Pt SAs and metallic Au NPs.

Catalysts with varying geometric structures were subsequently prepared, as shown in Figure 3c-g (the corresponding metal content was about 0.1 wt.% for SAs and 0.9 wt.%

15213773, Q. Downloaded from https://onlinelibrary.wiley.com/doi/10.1002/anie.202521118 by Cardiff University, Wiley Online Library on [24/11/2023]. See the Terms and Conditions (https://onlinelibrary.wiley.com/retrms-and-conditions) on Wiley Online Library for rules of use; OA articles are governed by the applicable Creative Commons Licenses

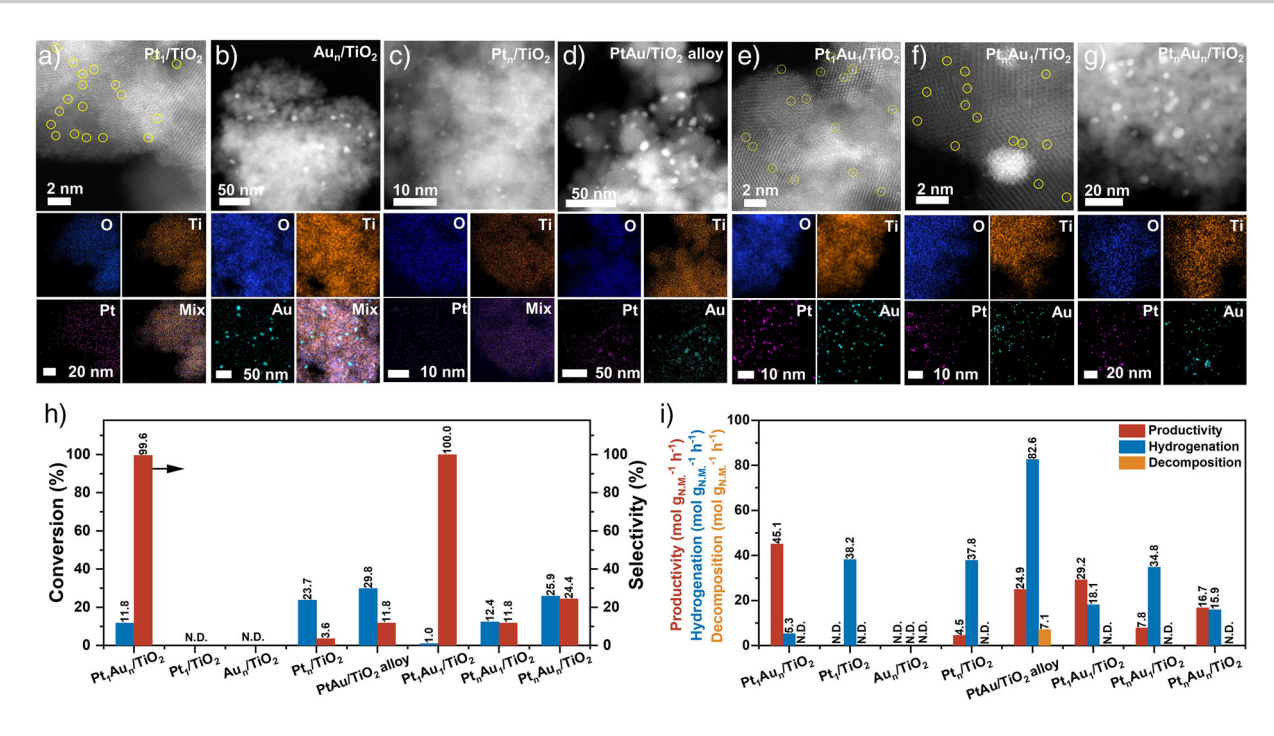


Figure 3. AC HAADF-STEM images and EDS mappings of a) Pt₁/TiO₂, b) Au_n/TiO₂, c) Pt_n/TiO₂, d) PtAu/TiO₂ alloy, e) Pt₁Au₁/TiO₂, f) Pt_nAu₁/TiO₂, and g) PtnAun/TiO2, single atoms are highlighted by the yellow circles; comparative. h) H2 conversion, H2O2 selectivity, and i) H2O2 productivity (reaction condition: 10 mL CH₃OH, 2.9 MPa 5% H₂/N₂, 1.1 MPa 25% O₂/N₂, T = 0 °C, 5 mg catalyst, 10 min, and stirring: 1200 rpm), hydrogenation (reaction condition: 0.25 mL 30 wt.% H₂O₂, 10 mL CH₃OH, 2.9 MPa 5% H₂/N₂, T = 0 °C, 5 mg catalyst, 10 min, and stirring: 1200 rpm), and decomposition (reaction condition: 0.25 mL 30 wt.% H₂O₂, 10 mL CH₃OH, 4.0 MPa N₂, T = 0 °C, 5 mg catalyst, 10 min, and stirring: 1200 rpm) on catalysts with different geometric structures.

for NPs, as reported in Tables S6 and S7). Interestingly, the Pt₁/TiO₂ catalyst, which consisted of atomic Pt species, was found to be inactive towards H₂O₂ synthesis, while the catalysts with Pt NPs (Pt_n/TiO₂, Pt_nAu₁/TiO₂, and Pt_nAu_n/TiO₂) offered only limited selectivities (< 25%, Figure 3h,i). On the other hand, the Au_n/TiO₂ catalyst (containing Au NPs) was inactive, presumably resulting from an inability to dissociate H₂, as indicated by the observation of no H₂ conversion over this formulation. Moreover, the PtAu/TiO2 alloy catalyst demonstrated a high H₂ conversion (29.8%), while its selectivity was only 11.8%, corresponding well with the observation of high H₂O₂ hydrogenation (82.6 mol·g_{N.M.}⁻¹·h⁻¹) and decomposition (7.1 mol· $g_{N.M.}^{-1}$ ·h⁻¹) activity. In contrast, no H₂O₂ degradation was observed for Pt₁Au_n/TiO₂ catalyst even at H₂O₂ concentrations as high as 14 wt.% (Figure S51). These results further revealed that the unique geometric structure of Pt SAs and Au NPs with close proximity was key to achieving efficient synthesis of H_2O_2 .

Unraveling the DSHP mechanism on Pt₁Au_n/TiO₂

In order to reveal the H₂ and O₂ activation mechanism over the reaction process, the H2 dissociation capacity of the Pt₁/TiO₂, Au_n/TiO₂, and Pt₁Au_n/TiO₂ catalysts was investigated using H_2 – D_2 exchange experiments (Figure 4a), which demonstrated that the Pt₁/TiO₂ formulations displayed a considerable HD signal at room temperature, indicating favorable H₂ dissociation capacity. Also, the Pt₁Au_n/TiO₂

catalyst showed a comparable H₂ dissociation capacity as Pt₁/TiO₂, whereas Au_n/TiO₂ showed no dissociation capacity for H₂. Subsequently, O₂-temperature programmed desorption (O2-TPD, Figure S52) was employed and in the case of the Pt₁/TiO₂ formulation revealed a distinct O₂ desorption peak at 463 °C, which was attributed to lattice O. By comparison, the Au-containing Au_n/TiO₂ and Pt₁Au_n/TiO₂ formulations not only displayed desorption peaks associated with lattice O, but also exhibited a desorption peak of chemisorbed O_2 at ~ 200 °C. [47] $^{16}O_2$ - $^{18}O_2$ exchange experiments further revealed that the Pt₁Au_n/TiO₂ (1.1E-8), as well as Au_n/TiO₂ (1.1E-8) and Pt₁/TiO₂ (1.1E-8) catalysts, displayed no dissociation ability for O₂ (1.1E-8 for blank, Figure \$53). Nevertheless, the Pt_n/TiO₂ exhibited an obvious ¹⁶O¹⁸O signal (1.5E–8), which revealed that the Pt NPs (i.e., Pt⁰) were capable of breaking O-O bonds, in agreement with experimental results, demonstrating that PtAu/TiO₂ catalysts consisting of Pt⁰ showed low H₂O₂ selectivity (the Pt_n/TiO₂, Pt_nAu₁/TiO₂, and Pt_nAu_n/TiO₂ catalysts offered selectivities of only 3.6%, 11.8%, and 24.4%, respectively, Figure 3h). The above results demonstrated that the separate Pt SAs and Au NPs were responsible for dissociative adsorption of H₂ and non-dissociative adsorption of O2, respectively.

Time-dependent in situ H2-O2-DRIFTS was employed to monitor the H_2 and O_2 activation process (Figure 4b-d). For the Pt₁Au_n/TiO₂ catalyst, following the introduction of O₂, weak peaks at 1221 and 814 cm⁻¹ were identified (the enlarged plot was displayed in Figure \$54), which corresponded to the vibrations of superoxo-like (*O₂)

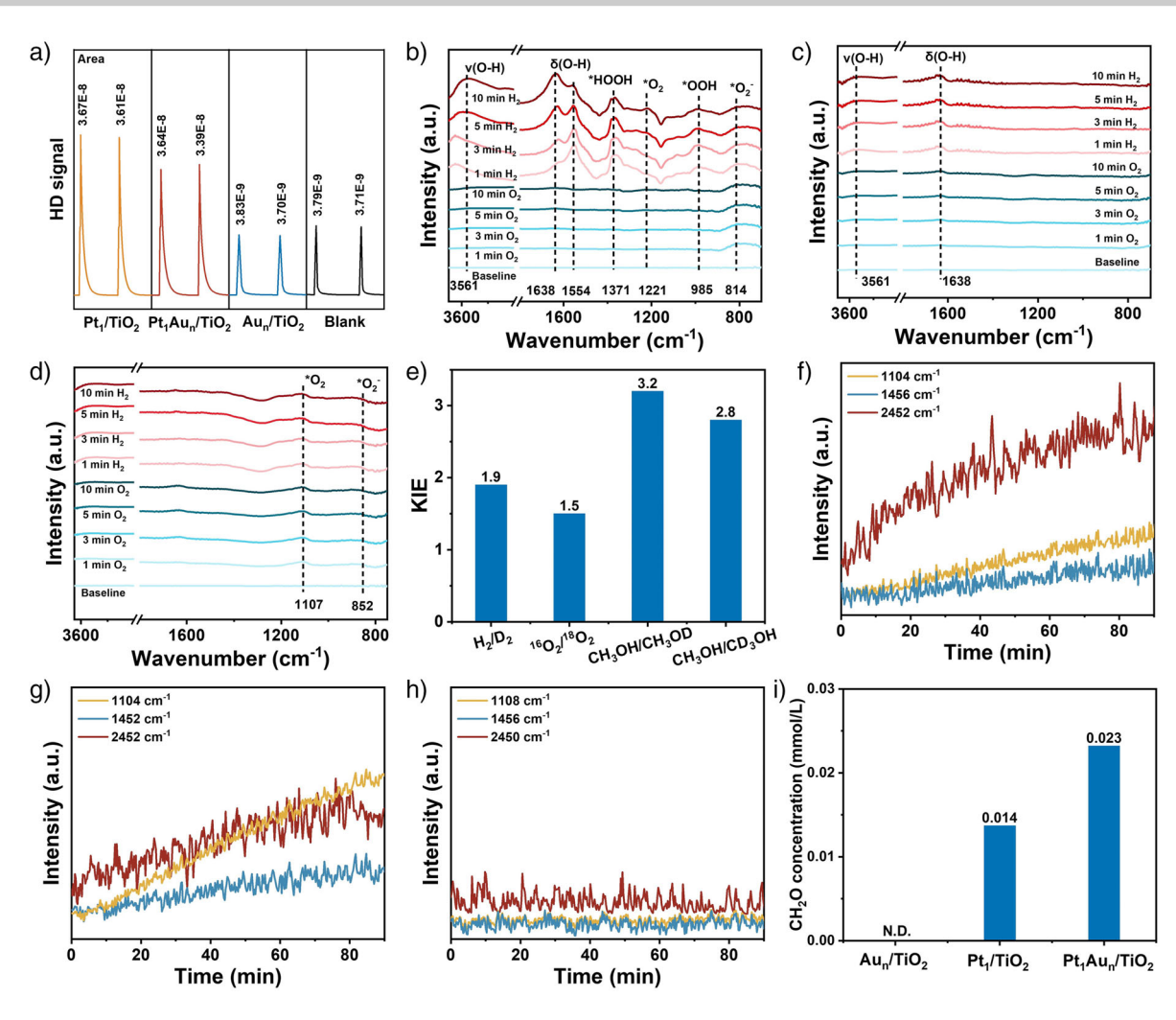


Figure 4. a) H_2-D_2 exchange experiments of Pt_1Au_n/TiO_2 , Pt_1/TiO_2 , and Au_n/TiO_2 at room temperature, 5% H_2/N_2 (30 mL/min) as carrier and D_2 (10 mL/min) as pulse gas, 1 mL quantitative ring, catalysts: 20 mg. Time-dependent in situ DRIFTS spectra of b) Pt_1Au_n/TiO_2 , c) Pt_1/TiO_2 , and d) Au_n/TiO_2 . e) Effects of isotopic substitution on rate constants. Peak trends at \sim 2450, \sim 1456, and \sim 1104 cm $^{-1}$ marked from the time-resolved operando infrared spectra with solvent subtraction on f) Pt_1Au_n/TiO_2 , g) Pt_1/TiO_2 , and h) Au_n/TiO_2 . i) The formaldehyde content of the post-reaction solution on Pt_1Au_n/TiO_2 , Pt_1/TiO_2 , and Au_n/TiO_2 . Reaction conditions: 10 mL CH₃OH, 2.9 MPa 5% H_2/N_2 , 1.1 MPa 25% O_2/N_2 , 0 °C, 5 mg catalyst, 30 min, and stirring: 1200 rpm.

adsorption and peroxo-like $(*O_2^-)$ configurations, respectively.[48,49] Then, with the introduction of H₂, new peaks corresponding to *OOH and *HOOH species were immediately recognized at 985 and 1371 cm⁻¹, respectively.^[50,51] Meanwhile, with the extension of H₂ exposure time, the intensities of the *O_2 and *O_2 peaks gradually diminished. This was likely due to the progressive conversion of adsorbed O2 into *OOH, while the further decrease in *OOH peak intensity can be attributed to subsequent transformation into *HOOH. However, there were no similar observations over the Pt₁/TiO₂ and Au_n/TiO₂ catalysts. Only the vibrational peaks of *OH were observed on Pt₁/TiO₂ with the introduction of H₂, while only the *O₂ and *O₂ peaks appeared on Au_n/TiO₂ with the introduction of O₂, further demonstrating that the separated H₂ and O₂ activation sites were located on Pt SAs and Au NPs, respectively.

To gain further insight into the mechanism of H₂ dissociation and proton-electron transfer to oxygen, we conducted

kinetic isotope experiments (Figure 4e). These experiments showed significant kinetic isotope effects (KIE) with values of 1.9 (H_2/D_2) and 1.5 ($^{16}O_2/^{18}O_2$), demonstrating that the kinetically significant interactions between intermediates containing active hydrogen and molecular oxygen were facilitated in the H₂O₂ formation process. Moreover, elevated CH₃OH-related KIEs (3.2 for CH₃OH/CH₃OD and 2.8 for CH₃OH/CD₃OH) suggested that the H species of O-H and C-H in CH₃OH may directly participate in the reaction. Time-resolved operando infrared spectra on Pt₁Au_n/TiO₂ (Figures 4f and S55) showed that the features at 1456 and 1104 cm⁻¹ identified as methyl and hydroxyl species, respectively, increased with time, evidencing the formation of η^2 -formaldehyde, which was regarded as a key species in H₂O₂ formation. In addition, the enhancement of the O-D peak at 2452 cm⁻¹ indicated a rapid exchange between -OD and -OH, with formaldehyde (CH₂O) acting as a hydrogen carrier (*CH₂OH) to transport hydrogen. Combining the 15213773, Q. Downloaded from https://onlinelibrary.wiley.com/doi/10.1002/anie.202521118 by Cardiff University, Wiley Online Library on [24/11/2023]. See the Terms and Conditions (https://onlinelibrary.wiley.com/retrms-and-conditions) on Wiley Online Library for rules of use; OA articles are governed by the applicable Creative Commons Licenses

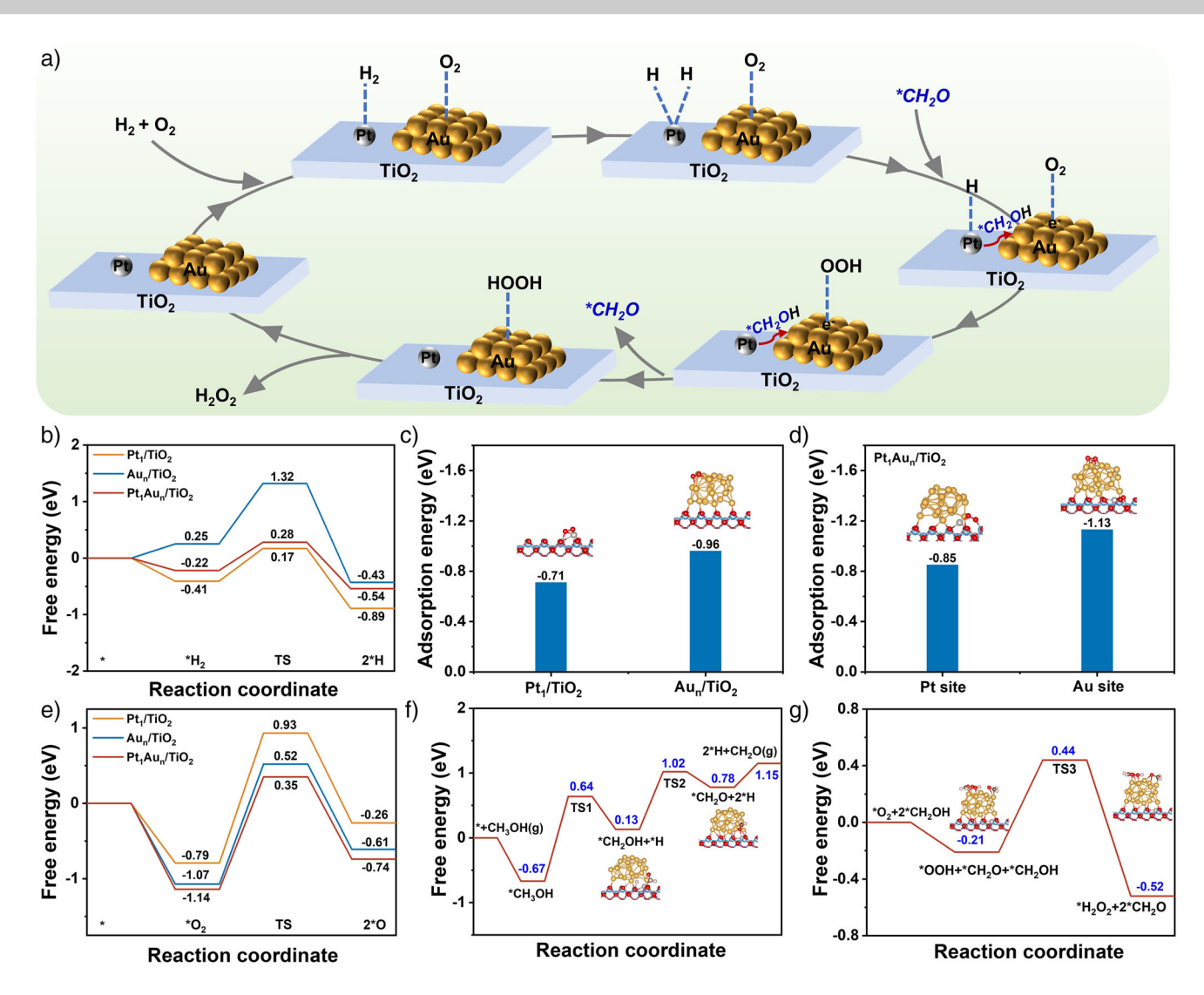


Figure 5. a) Scheme for the proposed reaction path on Pt_1Au_n/TiO_2 for direct synthesis of H_2O_2 . b) Free energy profiles for H_2 dissociation. c) O_2 adsorption energy on Pt_1/TiO_2 and Au_n/TiO_2 . d) O_2 adsorption energy on Pt_1Au_n/TiO_2 . e) Free energy profiles for H_2 dissociation. Free energy profiles for Pt_1Au_n/TiO_2 . The white, orange, red, pink, brownish, and light blue spheres represent Pt_1Au_1 , Pt_2Au_1 , Pt_3Au_2 , Pt_3Au_1 , Pt_3Au_2 ,

results of Figures 4g,h, and S55, CH₂O and O–D were formed on the Pt SAs. Figures S56–S59 showed that CH₃OH can be dehydrogenated to CH₂O in the presence of Pt₁Au_n/TiO₂ catalyst. Further, the CH₂O content of the post-reaction solution was also examined, and it was shown in Figure 4i that the CH₂O was only formed in the presence of Pt SAs (i.e., 0.014 and 0.023 mmol/L on Pt₁Au_n/TiO₂ and Pt₁/TiO₂, respectively), and not observed over the monometallic Au_n/TiO₂ catalyst, which was consistent with the infrared results (Figure 4f–h).

Based on these observations, we are able to propose the reaction pathway for DSHP over the Pt_1Au_n/TiO_2 formulation (Figure 5a). First, H_2 and O_2 were adsorbed on isolated Pt SAs and Au NPs (* + $H_2 + O_2 \rightarrow *H_2 + *O_2$), respectively, with * H_2 dissociated into two H⁺ (* $H_2 \rightarrow 2H^+ + 2e^-$). At the same time, CH₃OH was also dehydrogenated on Pt SAs to form *CH₂O. Subsequently, the dissociated H⁺, derived from H_2 , combined with the Au-adsorbed * O_2 to form *OOH

assisted by *CH₂O, which acted as a hydrogen carrier (H⁺ + e⁻ + *CH₂O + *O₂ \rightarrow *OOH + *CH₂O), after which the adsorbed hydroperoxy intermediate combined with the second H⁺ to form *H₂O₂ (H⁺ + e⁻ + *CH₂O + *OOH \rightarrow *HOOH + *CH₂O), and finally *H₂O₂ was desorbed to generate H₂O₂ (*HOOH \rightarrow H₂O₂ + *).

Theoretical Results

Density functional theory (DFT) calculations were conducted to further elucidate the underlying mechanism of H_2O_2 formation over the Pt_1Au_n/TiO_2 surface. According to the above catalyst characterizations, the Pt_1/TiO_2 catalyst was modeled with a Pt single atom anchored to the TiO_2 surface via oxygen bonds, while the Au_n/TiO_2 and Pt_1Au_n/TiO_2 systems were simulated by, respectively, loading Au_{21} clusters and co-anchoring an isolated Pt single atom with Au_{21} clusters

15213773, Q. Downloaded from https://onlinelibrary.wiley.com/doi/10.1002/anie.202521118 by Cardiff University, Wiley Online Library on [24/11/2023]. See the Terms and Conditions (https://onlinelibrary.wiley.com/etrms-and-conditions) on Wiley Online Library for rules of use; OA articles are governed by the applicable Cereaive Commons License

S60-S70.

on the TiO₂ surface. Specifically, the relative spatial position of Pt SAs and Au NPs in Pt₁Au_n/TiO₂ was spatially separated but adjacent. The models of these catalysts, including the

structures of major intermediates, were shown in Figures

Initially, we calculated the dissociation energy barrier of H₂ on Pt₁/TiO₂, Au_n/TiO₂, and Pt₁Au_n/TiO₂, respectively. As shown in Figure 5b, the H₂ adsorption occurred readily on Pt SAs over Pt₁/TiO₂ and Pt₁Au_n/TiO₂ with the free energy of -0.41 and -0.22 eV, respectively, whereas it was endothermic over Au_n/TiO_2 (0.25 eV). Moreover, the dissociation energy barriers of H₂ on Pt₁/TiO₂ (0.58 eV) and Pt₁Au_n/TiO₂ (0.50 eV) were notably lower than that of Au_n/TiO₂ (1.07 eV). These results indicated that both thermodynamically and kinetically, the activation of H₂ on Pt₁/TiO₂ and Pt₁Au_n/TiO₂ was favorable, consistent with the results of H₂-D₂ exchange experiments (Figure 4a). In the following, the non-dissociative adsorption energy results (Figures 5c.d) for O2 showed that O2 was more readily adsorbed on Au NPs (-0.96 and -1.13 eV over Au_n/TiO_2 and Pt_1Au_n/TiO_2 , respectively) than on Pt SAs (-0.71 and -0.85 eV) over Pt₁/TiO₂ and Pt₁Au_n/TiO₂, respectively). Moreover, within the Pt₁Au_n/TiO₂ catalyst, O₂ preferred to adsorb on Au NPs. The dissociation energy barriers of O2 (Figure 5e) on Pt₁/TiO₂, Au_n/TiO₂, and Pt₁Au_n/TiO₂ catalysts were as high as 1.72, 1.56, and 1.49 eV, respectively, indicating that O₂ was difficult to dissociate on these catalysts, which suppressed the side reaction of H₂ and O₂ to form water. Thus, it can be concluded from the above results that the Pt₁Au_n/TiO₂ catalyst exhibited both excellent H2 dissociation ability and non-dissociative adsorption capacity for O_2 .

The experimental results revealed that the dehydrogenation of CH₃OH to produce *CH₂O was a key step in the process of H₂O₂ formation over the Pt₁Au_n/TiO₂ catalyst. As shown in Figure 5f, the dehydrogenation process of CH₃OH occurs on Pt SAs verified by time-resolved operando infrared spectra (Figure 4f-h), and CH₃OH was easily adsorbed on Pt₁Au_n/TiO₂ with a free energy of -0.67 eV. However, the dehydrogenation of C-H in *CH₃OH (*CH₃OH → *CH₂OH + *H) required overcoming a significant energy barrier (1.31 eV), which was kinetically unfavorable, whereas the energy barriers (0.89 eV) for further dehydrogenation of *CH₂OH (*CH₂OH + *H \rightarrow *CH₂O + 2*H) were much lower, probably due to the more robust thermodynamic conditions provided when serving as an hydrogen carrier to transfer H and forming *OOH (free energy of -0.21 eV, $*O_2 + 2*CH_2OH \rightarrow *OOH + *CH_2O + *CH_2OH$, Figure 5g). The formation of *OOH not only consumed the *CH₂OH to drive the equilibrium from *CH₃OH to *CH₂OH in the forward direction, but also further lowered the dehydrogenation energy barrier of *CH₂OH on Pt SAs by generating *H₂O₂. The *OOH needed to overcome an energy barrier of 0.65 eV to react with *CH2OH to further form $*H_2O_2$ (*OOH + *CH₂O + *CH₂OH $\rightarrow *H_2O_2 + 2*CH_2O$). At the same time, *CH₂O was desorbed from the surface of the catalyst with a free energy of 0.37 eV (Figure 5f), which in turn generated *CH₂OH with the active hydrogen in the reaction to participate in the next catalytic cycle. Above dehydrogenation process of CH₃OH further demonstrated that *CH₂O acted as a hydrogen carrier bridge linking Pt SAs (H₂ dissociation sites) with Au NPs (O₂ adsorption sites).

Conclusion

In summary, we propose a novel strategy to construct efficient catalysts for DSHP that effectively decouple the two processes of H_2 and O_2 activation and elegantly assign them on distinct sites: Pt SAs for H_2 dissociation and Au NPs for O_2 non-dissociative adsorption. Under optimal conditions, the H_2O_2 productivity is comparable with that of the best Pd-based catalysts and significantly higher than that of reported non-Pd-based catalysts, with nearly 100% selectivity. A H_2O_2 concentration close to 4 wt.% can be achieved after sequential reactions, which is twice the initial concentration of the existing industrial approach to production. Extensive mechanistic studies directly indicate CH_3OH (the solvent in H_2O_2 formation) was dehydrogenated on Pt SAs to produce *CH_2O as an active hydrogen carrier, which subsequently combines with ${}^*O_2^-$ to produce H_2O_2 .

Supporting Information

The authors have cited additional references within the Supporting Information.

Acknowledgements

This work was supported by the National Key Research and Development Program Nanotechnology Specific Project (no. 2020YFA0210900), the National Natural Science Foundation of China (22422815, U22A20428), the Guangdong Natural Science Funds for Distinguished Young Scholar (2022B1515020035), the special fund for Science and Technology Innovation Teams of Shanxi Province (202304051001007). The authors thank the Guangdong Basic Research Center of Excellence for Functional Molecular Engineering, and the Chemistry and Chemical Engineering Guangdong Laboratory (grant no. 1922010). The authors also thank Dr. Rui Zhang and Mettler-Toledo for their analytical assistance and loan of the ReactIR equipment.

Conflict of Interests

The authors declare no conflict of interest.

Data Availability Statement

The data that support the findings of this study are available from the corresponding author upon reasonable request.

Keywords: Gold • Heterogeneous catalysis • Hydrogen peroxide • Platinum • Single atom catalysts

15213773, Q. Downloaded from https://onlinelibrary.wiley.com/doi/10.1002/anie.202521118 by Cardiff University, Wiley Online Library on [24/11/2025]. See the Terms and Conditions (https://onlinelibrary.wiley.com/terms-and-conditions) on Wiley Online Library for rules of use; OA articles are governed by the applicable Creative Commons Licensed

- S. J. Freakley, Q. He, J. H. Harrhy, L. Lu, D. A. Crole, D. J. Morgan, E. N. Ntainjua, J. K. Edwards, A. F. Carley, A. Y. Borisevich, C. J. Kiely, G. J. Hutchings, *Science* 2016, 351, 965–968, https://doi.org/10.1126/science.aad5705.
- [2] A. Huang, R. S. Delima, Y. Kim, E. W. Lees, F. G. L. Parlane, D. J. Dvorak, M. B. Rooney, R. P. Jansonius, A. G. Fink, Z. Zhang, C. P. Berlinguette, J. Am. Chem. Soc. 2022, 144, 14548–14554, https://doi.org/10.1021/jacs.2c03158.
- [3] C. Xia, Y. Xia, P. Zhu, L. Fan, H. Wang, Science 2019, 366, 226–231, https://doi.org/10.1126/science.aay1844.
- [4] S. Yu, X. Cheng, Y. Wang, B. Xiao, Y. Xing, J. Ren, Y. Lu, H. Li, C. Zhuang, G. Chen, *Nat. Commun.* 2022, 13, 4737, https://doi. org/10.1038/s41467-022-32450-6.
- [5] J. S. Adams, M. L. Kromer, J. Rodriguez-Lopez, D. W. Flaherty, J. Am. Chem. Soc. 2021, 143, 7940–7957, https://doi.org/10.1021/ iacs.0c13399.
- [6] D. W. Flaherty, ACS Catal. 2018, 8, 1520–1527, https://doi.org/10. 1021/acscatal.7b04107.
- [7] R. Ciriminna, L. Albanese, F. Meneguzzo, M. Pagliaro, ChemSusChem. 2016, 9, 3374–3381, https://doi.org/10.1002/cssc. 201600895.
- [8] A. G. Fink, R. S. Delima, A. R. Rousseau, C. Hunt, N. E. Lesage, A. X. Huang, M. Stolar, C. P. Berlinguette, *Nat. Commun.* 2024, 15, 766, https://doi.org/10.1038/s41467-024-44741-1.
- [9] M. Kou, Y. Wang, Y. Xu, L. Ye, Y. Huang, B. Jia, H. Li, J. Ren, Y. Deng, J. Chen, Y. Zhou, K. Lei, L. Wang, W. Liu, H. Huang, T. Ma, *Angew. Chem. Int. Ed.* 2022, 61, e202200413, https://doi.org/10.1002/anie.202200413.
- [10] C. Zhang, P. Shan, Y. Zou, T. Bao, X. Zhang, Z. Li, Y. Wang, G. Wei, C. Liu, C. Yu, Nat. Sustain. 2025, 8, 542–552, https://doi.org/10.1038/s41893-025-01538-4.
- [11] S. Shaybanizadeh, R. Luque, A. N. Chermahini, *Green Chem.* 2022, 24, 5524–5534, https://doi.org/10.1039/D2GC00918H.
- [12] Z. Yang, Z. Wei, S. Zhou, B. Bao, S. Zhao, F. Gong, Chem. Eng. J. 2023, 456, 140915, https://doi.org/10.1016/j.cej.2022.140915.
- [13] J. Chen, Q. Ma, Z. Yu, M. Li, S. Dong, Angew. Chem. Int. Ed. 2022, 61, e202213930, https://doi.org/10.1002/anie.202213930.
- [14] J. Wu, H. Xu, D. Cao, D. Cheng, J. Catal. 2024, 436, 115620, https://doi.org/10.1016/j.jcat.2024.115620.
- [15] H. Li, Q. Wan, C. Du, J. Zhao, F. Li, Y. Zhang, Y. Zheng, M. Chen, K. H. L. Zhang, J. Huang, G. Fu, S. Lin, X. Huang, H. Xiong, *Nat. Commun.* 2022, 13, 6072.
- [16] J. K. Edwards, B. Solsona, E. Ntainjua N, A. F. Carley, A. A. Herzing, C. J. Kiely, G. J. Hutchings, *Science* 2009, 323, 1037–1041, https://doi.org/10.1126/science.1168980.
- [17] G. V. Fortunato, E. Pizzutilo, I. Katsounaros, D. Gohl, R. J. Lewis, K. J. J. Mayrhofer, G. J. Hutchings, S. J. Freakley, M. Ledendecker, *Nat. Commun.* 2022, 13, 1973, https://doi.org/10.1038/s41467-022-29536-6.
- [18] A. Akram, G. Shaw, R. J. Lewis, M. Piccinini, D. J. Morgan, T. E. Davies, S. J. Freakley, J. K. Edwards, J. A. Moulijn, G. J. Hutchings, *Catal. Sci. Technol.* 2020, 10, 8203–8212, https://doi. org/10.1039/D0CY01163K.
- [19] R. Svensson, H. Grönbeck, J. Am. Chem. Soc. 2023, 145, 11579– 11588, https://doi.org/10.1021/jacs.3c00656.
- [20] C. Samanta, V. R. Choudhary, Catal. Commun. 2007, 8, 73–79, https://doi.org/10.1016/j.catcom.2006.05.027.
- [21] N. N. Edwin, M. Piccinini, J. C. A. Pritchard, J. K. Edwards, A. F. Carley, J. A. Moulijn, G. J. Hutchings, *ChemSusChem.* 2009, 2, 575.
- [22] T. Ricciardulli, S. Gorthy, J. S. Adams, C. Thompson, A. M. Karim, M. Neurock, D. W. Flaherty, J. Am. Chem. Soc. 2021, 143, 5445–5464, https://doi.org/10.1021/jacs.1c00539.
- [23] D. Kovačič, R. J. Lewis, C. M. Crombie, D. J. Morgan, T. E. Davies, Á. L. Martín, T. Qin, C. S. Allen, J. K. Edwards, L. Chen,

- M. S. S. Rasmussen, X. Liu, G. J. Hutchings, *Chem.* **2023**, *25*, 10436.
- [24] G. Jiang, L. Mou, Z. Wang, L. Zhang, T. Ji, L. Mu, J. Jiang, X. Lu, J. Zhu, ACS Catal. 2024, 14, 17055–17064, https://doi.org/10.1021/acscatal.4c04446.
- [25] Y. Zhang, Q. Sun, G. Guo, Y. Cheng, X. Zhang, H. Ji, X. He, Chem. Eng. J. 2023, 451, 138867, https://doi.org/10.1016/j.cej. 2022.138867.
- [26] Y. Liu, Z. Liu, J. Zhang, F. Xiao, X. Cao, L. Wang, Angew. Chem. Int. Ed. 2023, 62, e202312377, https://doi.org/10.1002/anje.202312377.
- [27] Y. Feng, Q. Shao, B. Huang, J. Zhang, X. Huang, Natl. Sci. Rev. 2018, 5, 895–906, https://doi.org/10.1093/nsr/nwy065.
- [28] G. M. Lari, B. Puertolas, M. Shahrokhi, N. Lopez, J. Perez-Ramirez, Angew. Chem. Int. Ed. 2017, 56, 1775–1779, https://doi.org/10.1002/anie.201610552.
- [29] E. Ye, F. Lin, C. Fu, X. Zhou, Q. Lin, H. Pan, Z. Chen, ACS Appl. Mater. Interfaces 2024, 16, 27490–27503, https://doi.org/10. 1021/acsami.4c05221.
- [30] J. Yoon, G. Han, M. Lee, S. Lee, S. Lee, K. Lee, Appl. Surf. Sci. 2022, 604, 154464, https://doi.org/10.1016/j.apsusc.2022.154464.
- [31] R. J. Lewis, M. Koy, M. Macino, M. Das, J. H. Carter, D. J. Morgan, T. E. Davies, J. B. Ernst, S. J. Freakley, F. Glorius, G. J. Hutchings, J. Am. Chem. Soc. 2022, 144, 15431–15436, https://doi.org/10.1021/jacs.2c04828.
- [32] J. M. Wei, S. Wang, J. G. Wu, D. Cao, D. J. Cheng, *Ind. Chem. Mater.* 2024, 2, 7–29, https://doi.org/10.1039/D3IM00054K.
- [33] M. J. Banisalman, H. W. Lee, H. Koh, S. S. Han, ACS Appl. Mater. Interfaces 2021, 13, 17577–17585, https://doi.org/10.1021/acsami.1c01947.
- [34] G. Li, J. Edwards, A. F. Carley, G. J. Hutchings, Catal. Today 2006, 114, 369–371, https://doi.org/10.1016/j.cattod.2006.02.070.
- [35] N. M. Wilson, Y. Pan, Y. Shao, J. Zuo, H. Yang, D. W. Flaherty, ACS Catal. 2018, 8, 2880–2889, https://doi.org/10.1021/acscatal. 7b04186.
- [36] D. Kim, H. Nam, Y. Cho, B. C. Yeo, S. Cho, J. Ahn, K. Lee, S. Y. Lee, S. S. Han, ACS Catal. 2019, 9, 8702–8711, https://doi.org/10.1021/acscatal.9b00451.
- [37] T. Ricciardulli, J. S. Adams, M. DeRidder, A. P. V. Bavel, A. M. Karim, D. W. Flaherty, *J. Catal.* 2021, 404, 661.
- [38] J. K. Edwards, J. Pritchard, L. Lu, M. Piccinini, G. Shaw, A. F. Carley, D. J. Morgan, C. J. Kiely, G. J. Hutchings, *Angew. Chem. Int. Ed.* 2014, 53, 2381–2384, https://doi.org/10.1002/anie. 201308067.
- [39] K. Cao, H. Yang, S. Bai, Y. Xu, C. Yang, Y. Wu, M. Xie, T. Cheng, Q. Shao, X. Huang, ACS Catal. 2021, 11, 1106–1118, https://doi. org/10.1021/acscatal.0c04348.
- [40] M. Selinsek, B. J. Deschner, D. E. Doronkin, T. L. Sheppard, J. Grunwaldt, R. Dittmeyer, ACS Catal. 2018, 8, 2546–2557, https://doi.org/10.1021/acscatal.7b03514.
- [41] J. S. Adams, A. Chemburkar, P. Priyadarshini, T. Ricciardulli, Y. Lu, V. Maliekkal, A. Sampath, S. Winikoff, A. M. Karim, M. Neurock, D. W. Flaherty, *Science* 2021, 371, 626.
- [42] W. Wang, S. Li, Q. Qiang, K. Wu, X. Pan, W. Su, J. Cai, Z. Shen, Y. Yang, C. Li, T. Zhang, *Angew. Chem. Int. Ed.* 2024, 63, e202404683, https://doi.org/10.1002/anie.202404683.
- [43] Z. Zhang, J. Tian, Y. Lu, S. Yang, D. Jiang, W. Huang, Y. Li, J. Hong, A. S. Hoffman, S. R. Bare, M. H. Engelhard, A. K. Datye, Y. Wang, *Nat. Commun.* 2023, 14, 2664, https://doi.org/10.1038/s41467-023-37776-3.
- [44] N. Huang, B. Li, D. Wu, Z. Chen, B. Shao, D. Chen, Y. Zheng, W. Wang, C. Yang, M. Gu, L. Li, Q. Xu, *Angew. Chem. Int. Ed.* 2024, 63, e202319177, https://doi.org/10.1002/anie.202319177.
- [45] A. I. M. Rabee, D. Zhao, S. Cisneros, C. R. Kreyenschulte, V. Kondratenko, S. Bartling, C. Kubis, E. V. Kondratenko, A. Brückner, J. Rabeah, *Appl. Catal. B: Environ.* 2023, 321, 122083, https://doi.org/10.1016/j.apcatb.2022.122083.





- [46] Y. Si, Y. Jiao, M. Wang, S. Xiang, J. Diao, X. Chen, J. Chen, Y. Wang, D. Xiao, X. Wen, N. Wang, D. Ma, H. Liu, Nat. Commun. 2024, 15, 4887, https://doi.org/10.1038/s41467-024-49083-6.
- [47] Y. Fang, Q. Zhang, H. Zhang, X. Li, W. Chen, J. Xu, H. Shen, J. Yang, C. Pan, Y. Zhu, J. Wang, Z. Luo, L. Wang, X. Bai, F. Song, L. Zhang, Y. Guo, Angew. Chem. Int. Ed. 2022, 61, e202212273, https://doi.org/10.1002/anie.202212273.
- [48] Y. Jiang, S. Li, S. Wang, Y. Zhang, C. Long, J. Xie, X. Fan, W. Zhao, P. Xu, Y. Fan, C. Cui, Z. Tang, J. Am. Chem. Soc. 2023, 145, 2698-2707, https://doi.org/10.1021/jacs.2c13313.
- [49] W. Ye, S. Chen, Y. Lin, L. Yang, S. Chen, X. Zheng, Z. Qi, C. Wang, R. Long, M. Chen, J. Zhu, P. Gao, L. Song, J. Jiang, Y. Xiong, Chem 2019, 5, 2865.
- [50] Y. Zhou, Y. Wu, Z. Luo, L. Ling, M. Xi, J. Li, L. Hu, C. Wang, W. Gu, C. Zhu, J. Am. Chem. Soc. 2024, 146, 12197–12205, https:// doi.org/10.1021/jacs.4c02986.
- [51] D. Jiao, C. Ding, M. Xu, X. Ruan, S. Ravi, X. Cui, Adv. Funct. Mater. 2025, 35, 2416753, https://doi.org/10.1002/adfm. 202416753.

Manuscript received: September 25, 2025 Revised manuscript received: October 25, 2025 Manuscript accepted: November 07, 2025 Version of record online: ■■, ■■

1521373 0, Downloaded from https://onlinelibrary.wiely.com/doi/10.1002/anie.202521118 by Cardiff University, Wiley Online Library on [24/11/2023], See the Terms and Conditions (https://onlinelibrary.wiely.com/retrms-and-conditions) on Wiley Online Library for rules of use; OA articles are governed by the applicable Creative Commons Licensed